J Mol Model (2011) 17:97–109
DOI 10.1007/s00894-010-0693-9

ORIGINAL PAPER

Computational characterization of how the VX nerve agent binds human serum paraoxonase 1

Steven Z. Fairchild · Matthew W. Peterson · Adel Hamza · Chang-Guo Zhan · Douglas M. Cerasoli · Wenling E. Chang

Received: 22 October 2009 / Accepted: 18 February 2010 / Published online: 9 April 2010

Abstract Human serum paraoxonase 1 (HuPON1) is an enzyme that can hydrolyze various chemical warfare nerve agents including VX. A previous study has suggested that increasing HuPON1's VX hydrolysis activity one to two orders of magnitude would make the enzyme an effective countermeasure for in vivo use against VX. This study helps facilitate further engineering of HuPON1 for enhanced VX-hydrolase activity by computationally characterizing HuPON1's tertiary structure and how HuPON1 binds VX. HuPON1's structure is first predicted through two homology modeling procedures. Docking is then performed using four separate methods, and the stability of each bound conformation is analyzed through molecular dynamics and solvated interaction energy calculations. The results show that VX's lone oxygen atom has a strong preference for forming a direct electrostatic interaction with HuPON1's active site calcium ion. Various HuPON1 residues are also detected that are in close proximity to VX and are therefore potential targets for future mutagenesis studies. These include E53, H115, N168, F222, N224, L240, D269, I291, F292, and V346. Additionally, D183 was found to have a predicted pKa near physiological pH. Given D183's location in HuPON1's active site, this residue could potentially act as a proton donor or accepter during hydrolysis. The results from the binding simulations also indicate that steered molecular dynamics can potentially be used to obtain accurate binding predictions even when starting with a closed conformation of a protein's binding or active site.

Keywords Binding · Homology model · HuPON1 · Steered molecular dynamics · Solvated interaction energy · VX

Electronic supplementary material The online version of this article (doi:10.1007/s00894-010-0693-9) contains supplementary material, which is available to authorized users.

S. Z. Fairchild (✉)
The MITRE Corporation,
7515 Colshire Drive,
McLean, VA 22102-7539, USA
e-mail: sfairchild@mitre.org

M. W. Peterson
The MITRE Corporation,
202 Burlington Road,
Bedford, MA 01730-1420, USA

A. Hamza · C.-G. Zhan
University of Kentucky College of Pharmacy,
725 Rose Street,
Lexington, KY 40536-0001, USA

D. M. Cerasoli
US Army Medical Research Institute of Chemical Defense,
3100 Ricketts Point Road,
Aberdeen Proving Grounds, MD 21010-5400, USA

W. E. Chang
The MITRE Corporation,
49185 Transmitter Road,
San Diego, CA 92152-7335, USA

Introduction

Organophosphorus nerve agents (OPNAs) such as soman, sarin, and VX are highly toxic compounds that irreversibly inhibit many serine esterases including acetylcholinesterase (AChE). Inhibition of AChE leads to increased levels of acetylcholine (ACh) at neuronal synapses, producing excessive muscle contractions that eventually cause death through asphyxiation [1]. While OPNAs were initially created and utilized for military applications, they have also been deployed by terrorist organizations [1]. A well-known example is the sarin gas attack in the Japanese subway system by members of the Aum Shinrikyo movement [2].

Treatments exist for exposure to OPNAs, but they have limited effectiveness. Anticholinergics counteract ACh's ability to stimulate smooth muscles [3], thereby helping block the effects of ACh accumulation. These can also be used in combination with oximes which help remove OPNAs from AChE's active site [3]. However, oximes are only effective if they are administered prior to OP aging. Carbamates are a pre-exposure option that reversibly inhibit a fraction of the AChE, thereby protecting it from deactivation by OPNAs. Carbamates can help protect against rapidly-aging OPNAs (e.g., soman), but they are not a substitute for other antidotes and are only effective if administered prior to OPNA exposure [3]. For severe poisonings, anticonvulsants can also be administered to reduce seizure activity [4]. Ultimately, each of these treatment options only masks the effects of OPNAs. No treatment that is currently fielded works by directly destroying OPNAs within the body.

An ideal treatment for OPNAs would rapidly eliminate nerve agents within the bloodstream rather than masking their effects. Enzymes specially designed to degrade OPNAs are one potential solution. These "OPases" would have the benefit of not only neutralizing OPNAs before they inhibit AChE, but would also provide a many-to-one effect where a single enzyme would eliminate numerous OPNA molecules. The enzymes would further have the benefit of being effective pre- and potentially post-exposure countermeasures and could also be deployed for decontamination purposes.

Human serum paraoxonase 1 protein (HuPON1) is a human hydrolase that could help combat OPNAs. HuPON1 is a 355-residue, 43-KDa protein that forms a six-fold β-propeller. The enzyme coordinates two calcium ions. One calcium ion is required for structural integrity while the other is required for catalytic activity [5]. The enzyme is synthesized and glycosylated in the liver then secreted into the bloodstream where it binds high-density lipoproteins (HDLs) [6]. HuPON1 possesses an inherent level of OPase activity [7], although this is considered secondary to its primary lactonase activity [8, 9]. A previous study has suggested that a ten-fold increase in HuPON1's OPase activity could make the enzyme a feasible countermeasure to OPNA exposure [10]. Additionally, previous studies have identified HuPON1 residues that are important for substrate interactions (L69, H115, H134, F222, L240, L267, D269, C284, H285, F292, T332, V346, and F347) and calcium coordination (E53, D54, N168, N224, D269, and N270) [11, 12].

An initial step to understanding how HuPON1 degrades OPNAs is determining HuPON1's three-dimensional structure. Currently, HuPON1's crystal structure has not been solved. However, a high-resolution structure of a gene-shuffled recombinant PON1 protein (rPON1) has been determined through X-ray crystallography (PDB ID: 1 V04) [13]. This structure contains two calcium ions and has a phosphate ion localized in the enzyme's putative active site. The bound phosphate is found to have one of its oxygen atoms forming an ionic interaction with the calcium ion required for catalytic activity. Further, the rPON1 structure is missing coordinates for residues 1–18 and 72–79 which were disordered in the crystal lattice [13]. The 83.7% sequence identity between rPON1 and HuPON1 makes rPON1 an excellent template for creating a 3-D model of HuPON1. Such homology modeling was recently performed using PSSP[12, 14]. However, other structure prediction packages such as I-TASSER [15, 16] and MODELLER [17, 18] can also be utilized to predict HuPON1's tertiary structure. Such studies would either verify the structure predicted by PSSP or offer alternate models for the missing loop regions of rPON1.

A second key to making HuPON1 an effective OPNA countermeasure is determining how the enzyme binds a given OPNA. Such information can be obtained through molecular docking software tools such as DOCK [19], AutoDock [20, 21], and FRED [22, 23]. These programs predict the most favorable binding conformations between small molecules and a target protein. The calculated binding energies can be well correlated with experimental results [24, 25] and can be utilized to re-engineer proteins [26]. For example, rPON1's enzymatic activity for different substrates was recently shown to be well correlated with predicted binding energies [27]. A drawback to the binding prediction programs is that they often have limited ability to model protein flexibility [28]. Molecular dynamics simulations of a bound complex can help overcome these inaccuracies, such as in solvated interaction energy (SIE) calculations [29, 30]. Additionally, techniques such as steered molecular dynamics (SMD) [31] can be utilized to simulate full protein flexibility during docking.

In this work, we characterize HuPON1's tertiary structure using two homology modeling methods (I-TASSER and MODELLER) with molecular dynamics refinement. Three static docking procedures (DOCK 6, AutoDock 4.0, and FRED) and SMD simulations are then used to find bound conformations of HuPON1 and VX. These conformations are further refined through molecular dynamics simulations. SIE is also utilized to calculate binding free energy estimates. The resulting bound structures enable identification and characterization of key enzyme-substrate interactions formed in the HuPON1-VX complex. The results also provide insight into a potential mechanism for HuPON1 hydrolysis of VX.

Methods

HuPON1 structure characterization

I-TASSER

HuPON1's structure was initially predicted using the I-TASSER server which obtained the most accurate results in

a recent CASP competition [16]. For the prediction, HuPON1's sequence was first extracted from GenBank [32] (accession number NM 000446). The sequence was then utilized as input for I-TASSER with all settings at default values. I-TASSER returned a structure built from all residues in rPON1's structure [13] and ab initio predictions for the missing loop regions (residues 1–15 and 72–79).

The structure from I-TASSER was then modified in four ways. First, the initial 18 residues were removed from the protein's N-terminal region. These residues are mostly hydrophobic and were predicted by I-TASSER to form an α-helix. Such a structure is consistent with a previous suggestion that these residues could form a transmembrane helix [13] that anchors HuPON1 to HDLs (in combination with other parts of HuPON1 [33]). Since simulations were performed without HDL present, this N-terminal anchoring region was not required. Second, calcium ions were added to the I-TASSER structure through alignment with rPON1. Third, sidechain protonation states were determined using the H++ webserver [34, 35]. Specifically, the initial I-TASSER structure was energy minimized in Amber [36] using the ff99SB force field [37] and generalized Born solvation [38, 39]. An H++ prediction was then run using a PQR file for the resulting structure with H++ settings at default values except the pH (which was set to physiological pH of 7.4). Final protonation states for histidine and cysteine residues were then determined through manual inspection. After setting the protonation states, the HuPON1 structure was energy minimized in Amber with TIP3P solvent [40] and neutralizing ions. The resulting structure was verified using PROCHECK [41, 42] and utilized as the starting point for the SMD simulations.

MODELLER

A second homology model of HuPON1 was created using MODELLER with independent modeling of the missing loop region. A multiple-sequence alignment was first performed with the "Homology" module of InsightII (Accelrys, Inc.) This returned rPON1 as the sole template. HuPON1's backbone structure was then generated from rPON1 using MODELLER. Sidechain conformations for conserved residues were set directly from rPON1, while side chain conformation for the non-conserved residues were generated using MODELLER's standard rotamer library[17, 18, 43].

Visual inspection of the rPON1 crystal structure revealed a three-fold rotational axis of symmetry (C3) orthogonal to the plane of the active site entrance. Each symmetrical unit contains two blades of HuPON1's 6-bladed β-propeller with an α-helix located between the second and third β-strands. The second missing loop region for rPON1 spans the region where an α-helix is formed in the other two symmetrical units. Given this symmetry, the missing loop region was built based on the other two symmetric units. Specifically, the structures for residues 183–202 (loop 2) and 283–302 (loop 3) were used to model residues 66–85 (loop 1). Note that five residues on either side of rPON1's second missing loop region (residues 66 to 72 and 80 to 85) were used in building the model for loop 1. This was done to provide better structural agreement with loops 2 and 3. The structures for loops 2 and 3 were initially fit to loop 1 through RMSD minimization.

After RMSD minimization, the resulting structures were refined in MODELLER with sidechain conformations determined from the standard residue library. Of the top 25 structures returned by MODELLER, the one with the best probability score was utilized for further refinement. For this structure, sidechain protonation states were set so that all aspartic acid and glutamic acid residues had a charge of negative one, all lysine and arginine residues had a charge of plus one, and all histidine residues were neutral. The sidechain nitrogen atom that was protonated for each histidine was determined through manual inspection of the protein's structure. The structure was then energy minimized in Amber using explicit TIP3P solvation and the ff99 [44] force field. The final structure was verified with PROCHECK and utilized for the DOCK, AutoDock, and FRED binding simulations.

VX structure

All studies were performed using the neutral S isomer of the VX nerve agent [(S-[2-(diisopropylamino)ethyl]-O-ethyl methylphosphonothioate)]. This isomer was selected due to its higher reactivity toward human AChE compared to the R isomer (115 fold greater reactivity in a recent study [45]).

The VX structure utilized for the DOCK, AutoDock, and SMD simulations was obtained by converting VX's simplified molecular input line entry specification (SMILES) [46] into protein data bank (PDB) format through an online SMILES converter [47]. The Amber molecular modeling package [36] was then utilized to determine the resulting molecule's AM1-BCC charges [48, 49] and subsequently equilibrate the molecule to physiological conditions (300 K and 1 atmosphere) in explicit TIP3P solvation. The entire system was then energy minimized, and VX's coordinates extracted from the energy-minimized system.

The VX molecule utilized for FRED docking simulations and subsequent MD analysis was found through ab initio electronic structure calculations using the Gaussian03 program [50] at the HF/6-31G* level. The optimized geometry was used to calculate the molecular surface electrostatic potentials at the same HF/6-31G* level, and the potentials were then utilized to determine partial atomic

charges through restrained electrostatic potential fitting [51, 52]. These charges were used for VX atoms during both FRED docking and subsequent MD simulations. Missing force field parameters for VX were set using the General Amber force field [53].

Binding simulations

AutoDock

For the AutoDock binding simulations, atom types and Gasteiger [54, 55] charges were determined for HuPON1 and VX using the AutoDockTools toolkit [56]. The sampling grid had a resolution of 0.375 Å with 40 points in each direction and was centered on residues F222, N224, L240, H285, F292, and V346. AutoDock was run using the Lamarckian genetic algorithm (LGA) and empirical energy function [21]. The initial population size was 300, and the maximum number of energy evaluations was 2.5×107. Default options were utilized for the pseudo-Solis and Wets local search. HuPON1 was kept rigid during the docking process, while VX was treated as flexible. We ran 100 independent iterations of the LGA, and clustering was performed with a RMS tolerance of 1.5 Å. The lowest energy conformation from the top scoring cluster was then Aquilibrated through molecular dynamics utilizing the procedure listed in the "Solvated Interaction Energies" section.

DOCK

For DOCK, we prepared the HuPON1 and VX molecules for docking with the UCSF Chimera application [57]. HuPON1's partial atomic charges were assigned using the ff99SB force field [37], and VX's partial atomic charges were assigned using AM1-BCC [48, 49]. The molecular surface was calculated using the dms program, an implementation of the Lee and Richards algorithm [58]. SPHGEN was used to calculate the spheres representing a negative image of the receptor, and those spheres within 15 Å of the active site calcium were used to generate the grid. Flexible docking was performed using the anchor- and -grow method with a minimum anchor size of 6 atoms and a maximum of 1000 conformations. Clustering was performed with an RMS tolerance of 1.5 Å. The lowest energy conformation (by the dock6 grid scoring function) from the top scoring cluster was then equilibrated through molecular dynamics using the procedure listed in the "Solvated Interaction Energies" section.

FRED

Docking with the FRED software package [22, 23] consisted of an initial shape fitting process followed by optimization. During shape fitting, different ligand conformations were tested within a grid box that encompassed all active-site atoms and had a resolution of 0.5 Å. Two optimization filters were applied that accounted for favorable rigid-body interactions and ligand dihedral angles. The largest resulting cluster had VX's lone oxygen interacting with HuPON1's active site Ca^{2+}. Since a similar interaction was observed for the phosphate in rPON1's X-ray structure [13], only bound conformations were retained that had this interaction. Each structure in the top scoring cluster was then simulated through MD in Amber using an in vacuo potential with a non-bonded cutoff of 20 Å and a dielectric constant of $\epsilon=4$ r [59, 60]. The resulting pose with the best interaction energy was further refined through MD simulations with explicit TIP3P solvation and neutralizing sodium ions. The initial system was first energy minimized, and MD simulations were then performed using a method similar to previous studies [61–63]. Specifically, 200 ps of MD simulations were performed without any constraints followed by 5 ns of MD simulations with harmonic constraints of 25 kcal/(Å^{2}mol) applied to all α-carbons. The constraints helped prevent changes in HuPON1's structure in the high B-factor regions (e.g., loops near the active site). The final equilibrated conformation was taken as the bound HuPON1-VX structure.

Steered molecular dynamics

Binding simulations were also performed through SMD. The initial system was created by aligning VX directly in front of HuPON1's active site in Swiss-PdbViewer [64]. This starting conformation had VX's phosphorus, sulfur, and nitrogen atoms at 33.5 Å, 32.6 Å, and 34.1 Å from the active site calcium ion, respectively. The entire system was then energy minimized, temperature equilibrated to 300 K over 10 ps, and pressure equilibrated to 1 atm over 100 ps. The coordinates for HuPON1 and VX were harmonically constrained during both the temperature and pressure equilibrations using a force constant of 10 kcal/(Å^{2}mol). This was followed by ten independent simulations that were each run for 1 ns without any atomic constraints. From these ten simulations, a structure was selected with VX just outside of HuPON1's active site. This structure was then used for SMD simulations where VX's phosphorus, sulfur, and nitrogen atoms were driven from their starting positions to within either 3 Å or 5 Å of HuPON1's active site calcium ion (six total simulation types). This tested different methods of VX entry into HuPON1's active site. The SMD simulations each ran for 1 ns with a driving force constant of 10 kcal/(Å^{2}mol). Each simulation was repeated five times, and the final conformation for each run was simulated for 2 ns without system constraints to test for stability of the HuPON1-VX interaction.

Solvated interaction energies

We utilized the SIE method [29, 30] to further characterize the binding interactions of the different HuPON1-VX complexes. SIE is a procedure that can estimate protein-ligand binding free energies using independent samples from a molecular dynamics simulation. Like the molecular mechanics Poisson-Boltzmann surface area approach [65], SIE combines intermolecular interaction terms (electrostatic and van deer Waals) with solvation free energy terms in determining binding free energies. However, unlike MM-PBSA, the SIE approach has been optimized to match a range of known protein-ligand binding energies [29]. Trajectories for the SIE calculations were generated using the Amber molecular modeling package. All simulations were performed using the ff99SB force field with explicit TIP3P solvent and neutralizing sodium ions. The simulations also used the SHAKE algorithm with a 2 fs time step. The system was first energy minimized for 1000 cycles then heated from 0 K to 300 K over 50 ps using a Langevin thermostat. During the heating process, the protein and calcium ion Cartesian coordinates were harmonically constrained with a force constant of 2 kcal/(Å^{2}mol). The system was then pressure equilibrated for 50 ps under the same restraints. Next, the restraints were removed, and the system was allowed to equilibrate for 1.5 ns. Finally, the equilibrated system underwent a 2 ns production run with snapshots saved at 2 ps intervals. The 1000 snapshots were then utilized for calculating the SIE binding energy.

Computational solvent mapping

The FTMAP server [66] was used to perform computational solvent mapping analysis [67] on the MODELLER-based HuPON1 structure. This technique involves finding favorable binding orientations for small molecules on the target protein and then clustering the molecules based on location. Larger clusters have been shown to correspond to a protein's active/binding sites [68]. The method also returns a count for how many nonbonded interactions and hydrogen bonds are formed between each residue and the bound organic molecules.

Key residue identification

Key HuPON1 residues that interact with VX in each bound structure were detected by calculating the distance between all HuPON1 and VX atoms. Any HuPON1 residue that had at least one atom (including hydrogen) within 3 Å of any VX atom was indicated as interacting with VX. Key residues were detected utilizing the bound VX conformations predicted by DOCK, AutoDock, FRED, and SMD in Amber.

Results and discussion

HuPON1 structure

Two 3-D models were created for HuPON1. One structure was generated using the I-TASSER homology modeling server. The second structure was generated using MODELLER with independent modeling of residues 66 through 85. Comparisons were then made between the two predicted structures and a recently published HuPON1 structure generated using PSSP [12].

The HuPON1 structures from I-TASSER, MODELLER, and PSSP were found to be equivalent except near the missing loop region of rPON1. Specifically, the three structures have α-carbon RMSDs of 0.37 Å, 0.15 Å, and 0.13 Å, respectively, to rPON1 across all residues except the first 18 and those surrounding the missing loop region (residues 69 through 82). Different conformations for the missing loop region are illustrated in Fig. 1a. As the figure

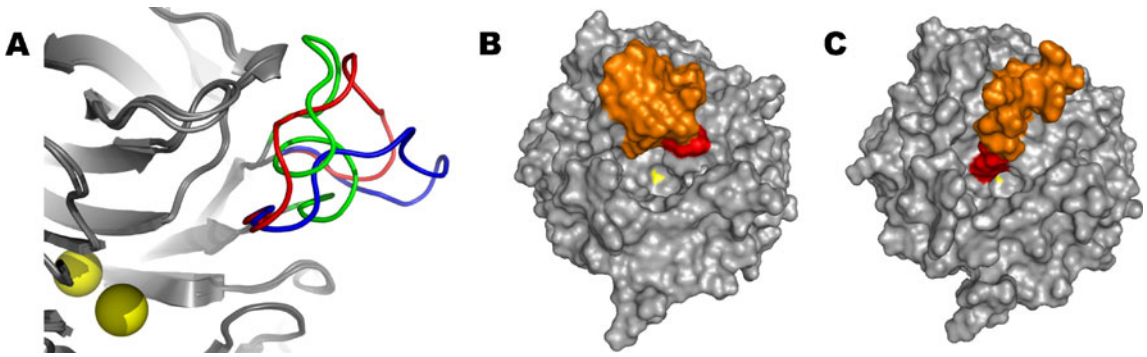

Fig. 1 Comparison of differences between the HuPON1 homology models for the missing loop residues of rPON1. The left image (**a**) shows residues 69 through 82 in different colors for the I-TASSER (blue) and MODELLER (green) structures generated in this study along with the PSSP (red) structure which was generated in a separate study [12]. Calcium ions are drawn as yellow spheres. The middle and right figures illustrate differences in the HuPON1 active site for the MODELLER and I-TASSER structures, respectively. Residues 66 through 85 are highlighted in orange, residue Y71 is drawn in red, and the active site calcium is shown in yellow. All images were created in PyMOL [72]

shows, the I-TASSER-based and PSSP-based structures are similar. Both extend upward along the main β-barrel axis before bending at residue P72 and moving outward toward the protein's exterior. The structures then cut back along the protein's exterior toward the intersection between β-blades 1 and 6 before forming a turn near residue P79 and looping back to join the main protein structure. The MODELLER-based structure is significantly different. It has a loop that extends directly out from the second β-strand before forming a short α-helical coil between G73's carboxyl group and N78's amide group. A random coil region then extends toward the protein's exterior and connects the α-helix back to the main protein body.

It was also found that the different conformations for the missing loop region result in significant structural differences near HuPON1's active site. As shown in Fig. 1b, the MODELLER-based structure has an open active site which would enable VX to easily access HuPON1's active site calcium. On the other hand, Fig. 1c shows that the missing loop region of the I-TASSER structure extends into HuPON1's site and has Y71's hydroxyl sidechain group interacting with the active site calcium ion. This interaction causes Y71's phenol group to effectively block HuPON1's active site.

Gauging which computational model best represents HuPON1's structure under physiological conditions is nontrivial. The fact that PSSP and I-TASSER returned similar structures argues for this conformation. However, the short α-helix in the MODELLER-based structure matches α-helices found on β-blades 3 and 5, giving the protein an overall three-fold symmetry. Additionally, given the missing loop region's high flexibility, HuPON1's range of thermodynamic motion may span all three predicted structures. Ultimately, determining which structure best represents the missing loop region will require further experimental data. In the absence of such information, we view all three models as potential HuPON1 structures. However, given that Y71 is blocking the active site in the I-TASSER structure, it is not expected that static binding to this conformation will provide meaningful results. Therefore, the MODELLER-based structure was utilized for all static binding simulations. The I-TASSER-based structure of HuPON1 was utilized for SMD simulations to test if SMD can find stable binding predictions when starting with a closed conformation of the enzyme's active site.

Regarding protonation states, the sidechain proton locations for all histidine residues were determined through energy calculations and manual inspection of local environments. The following residues were predicted to have a proton located on the δ nitrogen: H115, H134, H184, H243, H251, and H348. All other histidine residues had the proton located on the ϵ nitrogen. As in rPON1, a disulfide bridge was found between C42 and C353. For the remaining ionizable groups, H++ predicted most sidechains to be in the expected protonation state at pH=7.4. The one exception was D183's sidechain carboxyl group which had a predicted pKa of 10.05. In the I-TASSER structure, this residue is solvent exposed in HuPON1's active site and is situated ~6 Å from the active site calcium ion. Placing H184's proton on the nitrogen slightly increases D183's predicted pKa to 10.84. Additionally, modeling H134 in the dual protonated (positively charged) state and H115 in the ϵ-protonated state (i.e., the state after H115 has accepted a proton) causes D183 to have a predicted pKa of 7.85. Thus, D183 is expected to exist predominantly in the protonated state for the I-TASSER structure. Given its location and range of predicted pKa values, D183 could very well serve as a proton donor or acceptor in HuPON1 hydrolysis reactions.

Bound VX structures

Bound conformations of VX in HuPON1's active site were obtained through AutoDock, DOCK, FRED, and SMD simulations. The AutoDock, DOCK, and FRED bound conformations were all generated using the MODELLER-based HuPON1 structure, while the SMD results were obtained with the I-TASSER-based structure. All bound conformations were equilibrated through molecular dynamics, and the final conformation from the simulation was utilized as the bound structure for each docking method.

Figure 2 compares the final bound VX conformations across the four different binding procedures tested with all bound conformations aligned to rPON1 (for comparing VX orientations). Individual results are shown in Fig. 2a–d, and all four structures are superimposed in Fig. 2e. As the images demonstrate, the lone oxygen on VX's phosphorus atom interacts directly with the active site calcium ion in all four predicted binding conformations. Similar interactions have been predicted for binding studies with other substrates of HuPON1 [12, 69]. This interaction is reasonable since it would help pull electrons from VX's phosphorus atom and facilitate nucleophilic attack on the phosphorus by an electronegative atom.

Figures 2a–d also show that VX can still have a range of orientations in HuPON1's active site even with anchoring of the lone oxygen to the active site calcium. The DOCK and SMD structures are nearly identical, with each placing N224's sidechain oxygen next to VX's phosphorus atom along the phospho-sulfur (P-S) bond. These results are encouraging since the two bound conformations were generated using different docking procedures and different models of HuPON1's structure. Figure 2c shows that the FRED-based structure has VX rotated ~90° counterclockwise along the torsional axis going from VX's lone oxygen atom to the active site calcium ion. This puts residue D269 near the phosphorus atom directly behind VX's P-S bond.

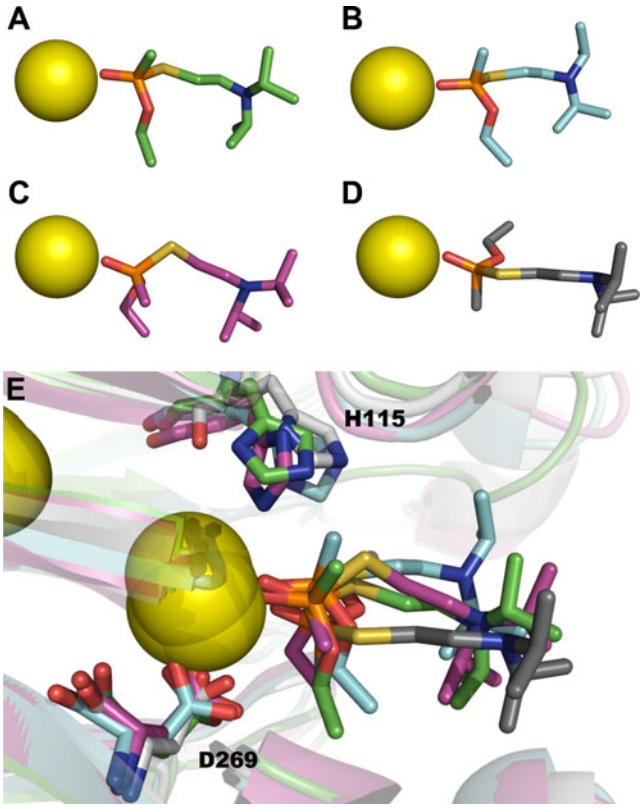

Fig. 2 Bound VX conformations found by steered molecular dynamics (**a**), DOCK (**b**), FRED (**c**), and AutoDock (**d**). Image E shows the superposition of all four bound VX conformations. Residues H115 and D269 are illustrated as stick diagrams to demonstrate relative orientation of the bound conformations within HuPON1's active site. The surrounding protein is drawn as a semi-transparent ribbon, and the bound calcium ions are depicted as yellow spheres. Carbon atom colors indicate the docking method utilized: green = SMD, blue = DOCK, purple = FRED, and gray = AutoDock. Other atom colors are blue for nitrogen, yellow for sulfur, orange for phosphorus, and pink for oxygen. Image generated in PyMOL [72]

Finally, Fig. 2d shows that the AutoDock conformation is rotated an additional 90° counterclockwise along the P-Ca^{2+} torsional axis relative to the FRED structure, placing residue E53 next to VX's phosphorus atom along the P-S bond.

Altogether, the bound conformations illustrate that VX's lone oxygen atom likely forms a direct interaction with the active site calcium ion. The results also indicate that various rotations of this bound conformation are predicted to be energetically favorable within HuPON1's active site. This may be due to some binding predictions being inaccurate, or may reflect a range of possible conformations for VX within the active site which are all tenable under physiological conditions.

SMD simulations

The SMD simulations performed in this study tested if SMD can obtain predictions of how HuPON1 binds VX when starting with a closed conformation of HuPON1's active site. As illustrated in Fig. 3a, the initial I-TASSER prediction for HuPON1 has residue Y71 blocking a significant portion of HuPON1's active site. Figure 3b shows the active site after the SMD simulation including the predicted binding conformation of VX. As is apparent, significant changes to the active site occurred during the binding simulation. In particular, Y71 has moved away from the active site, resulting in a pocket that is large enough to facilitate VX interacting directly with the active site calcium ion. Given that Y71 is part of the disordered loop in rPON1's X-ray structure, these results indicate that the flexible loop region may act as a gatekeeper with Y71's position determining whether or not substrates can bind. These findings are consistent with "open-closed" conformational changes observed for HuPON1 in previous MD simulations [12]. The fact that the SMD binding predictions with a closed HuPON1 conformation match static binding predictions with

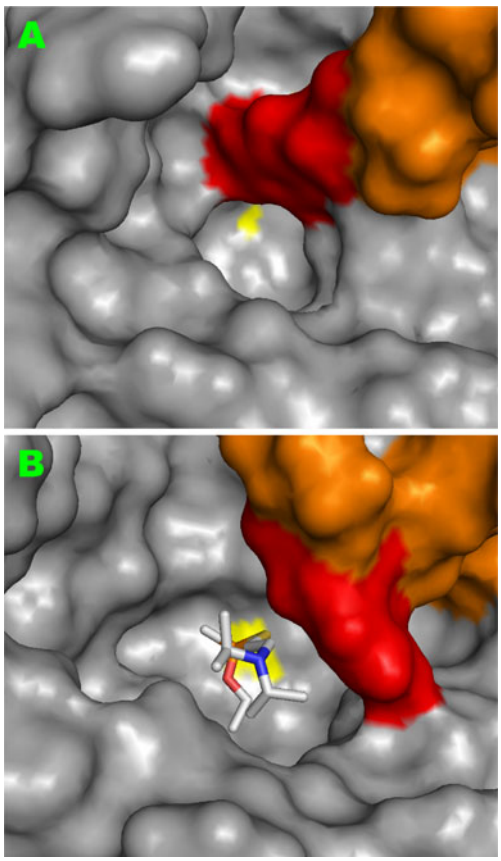

Fig. 3 HuPON1's active site before and after SMD binding simulations. The top figure (**a**) shows the active site for the initial I-TASSER prediction for HuPON1's structure. The calcium ion is drawn in yellow, Y71 in red, and residues 69 through 82 in orange. For this structure, the hydroxyl group on Y71's sidechain interacts with the active site calcium causing blockage of HuPON1's active site. The bottom figure (**b**) shows the conformation of HuPON1 after running SMD binding simulations. Here, residue Y71 is repositioned so that VX (stick diagram) can bind HuPON1's active site. Images generated in PyMOL [72]

an open HuPON1 conformation suggests that SMD can obtain accurate binding predictions even when starting with a 'closed' protein structure. Therefore, SMD-based binding predictions could be especially useful for protein-ligand or enzyme-substrate systems where the protein structure is solved in the absence of a ligand or substrate analog."

Computational solvent mapping

The FTMAP server detects where small inorganic materials interact favorably with a protein, helping locate likely binding/active sites. An initial FTMAP analysis of HuPON1 revealed two major clusters of inorganic molecules. One cluster was located in HuPON1's active site, while the other (larger) group was on the opposite side of the protein. To obtain results for only HuPON1's active site, a second FTMAP analysis was performed with a mask applied to the second binding site. Figure 4 shows the resulting small molecule clusters from the second analysis. As the figure demonstrates, the small molecules all cluster in HuPON1's active site close to the catalytic calcium ion.

We continued the FTMAP analysis by determining the percentage of non-bonded and hydrogen-bonded interactions formed by each of HuPON1's active site residues. The following residues were found to independently account for over 5% of all non-bonded interactions with the small molecules: H115, D183, H184, F222, I291, and F292. Meanwhile residues K75, N113, P114, N166, D183, Q192, D269, H285, I291, and V346 independently account for over 5% of all hydrogen-bonds. Across these residues, I291 is the only residue that accounts for over 10% of both non-bonded and hydrogen-bonded interactions (11.8% and 13.9%, respectively), indicating I291 is likely important for substrate recognition and binding. FTMAP also identified H115, F222, and D269 as residues which may have roles in substrate binding. Previous studies have shown HuPON1 may have different enzymatic mechanisms for different substrates [70]. Thus, some residues identified through the FTMAP analysis may be required for hydrolyzing one family of molecules but not another. Figure 4 shows that the predicted binding conformation for VX is in good agreement with many small molecule binding sites predicted by FTMAP.

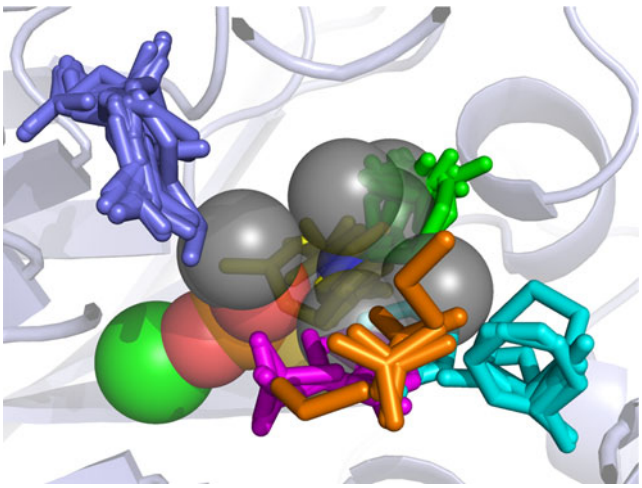

Fig. 4 FTMAP[66] prediction of solvent binding locations for the MODELLER-based HuPON1 structure. Solvent molecules are drawn as sticks and colored by cluster. The AutoDock4-based bound conformation for VX is drawn using semi-transparent spheres and gray carbon atoms. The active site calcium ion is shown as a green sphere. Image generated in PyMOL [72]

Key residue detection

To further characterize which key residues interact with VX, all residues were identified that have at least one atom within 3 Å of any VX atom in each bound conformation (including hydrogens). The resulting residues are listed in Table 1. Selecting those residues where at least three of four binding procedures place the residue within 3 Å of VX gives the following set: E53, H115, N168, F222, N224, L240, D269, I291, F292, and V346. The locations of these residues are depicted in Fig. 5 for the various predicted binding conformations of HuPON1 and VX.

Key residue interactions

DOCK

The contacts for residues in Table 1 were visually examined for each bound structure. In the bound DOCK conformation, the sidechains of residues E53, N168, N224, and D269 along with the backbone oxygen of N224 all help coordinate the active site calcium ion. Residues K75, H115, F292, V346, and F347 interact with VX's hydrophobic (diisopropylamino)ethyl (DPAE) group at or past VX's sulfur atom. H115, which has been proposed as a catalytic residue [13], is located near VX's sulfur opposite the phosphorus atom along the P-S bond. Thus H115 is not positioned to coordinate a water-based SN2 attack of VX's P-S bond at the phosphorus atom. However, H115 is positioned to potentially serve as a proton donor to the sulfur atom. For the remaining residues, I291 and L240 interact with VX's O-ethyl group, while F222 is found near the methyl moiety on VX's phosphorus atom.

Steered molecular dynamics

The HuPON1-VX complex determined through SMD is similar to that determined by DOCK but with minor differences. As with DOCK, E53, D269, and N224 all coordinate the active site calcium ion. However, N224 only

Table 1 Key HuPON1 residues. HuPON1 residues near VX were identified using AutoDock4 (AD), DOCK, FRED, and steered molecular dynamics in Amber (SMD). Residues receive a score of 1 if they have one atom within 3 Å of any VX atom (including hydrogens). 'Ca2+' implies the residue coordinates the active site calcium, 'DPAE' represents an interaction with VX at the (diisopropylamino)ethyl group, 'P-S' represents an interaction along VX's P-S bond, and 'O-ethyl' and 'Methyl' represent interactions with groups attached to VX's phosphorus atom. The different bound structures are signified with ^{D} for DOCK, ^{A} for AutoDock, ^{F} for FRED, and ^{S} for SMD

Residue	AD	FRED	DOCK	SMD	Σ	Interaction
E53	1	1	1	1	4	Ca2+^{A,D,F,S},O-ethyl^{A}
Y71	1	0	0	1	2	DPAE^{S}, O-ethyl^{A}
K75	0	0	1	0	1	DPAE
H115	1	1	1	1	4	DPAE^{D},O-ethyl^{A} P-S^{F,S}
N168	0	1	1	1	3	Ca2+^{D,F}, Methyl^{S}
H184	1	0	0	0	1	DPAE
M196	1	0	0	0	1	DPAE
F222	1	1	1	0	3	DPAE^{A,F}, Methyl^{F,D}
N224	0	1	1	1	3	Ca2+
L240	1	1	1	1	4	DPAE^{A}, Methyl^{F}, O-ethyl^{D,S}
L241	1	0	0	0	1	DPAE
D269	1	1	1	1	4	Ca2+
H285	0	1	0	0	1	O-ethyl
I291	1	1	1	1	4	DPAE^{A,F,S}, O-ethyl^{F,D}
F292	1	1	1	1	4	DPAE
T332	1	1	0	0	2	Methyl^{A}, O-ethyl^{F}
V346	1	1	1	0	3	DPAE^{D}, Methyl^{A}, O-ethyl^{A,F}
F347	0	0	1	0	1	DPAE

coordinates the ion with its sidechain (and not its backbone). Additionally, N168 does not coordinate the calcium ion but instead interacts with VX's O-ethyl group. Additionally, Y71, I291, and F292 interact with VX's DPAE moiety (rather than K75, H115, F292, V346, and F347). As with the DOCK structure, H115 is again found near VX's sulfur atom. However, for the SMD-based structure, H115's sidechain is between the P-S bond opposite the O-ethyl moiety. This geometry also would not facilitate an SN2 attack of the P-S bond by a water molecule coordinated by H115. Instead, N224 is found closest to the phosphorus atom along VX's P-S bond. Lastly, L240 interacts with VX's O-ethyl group.

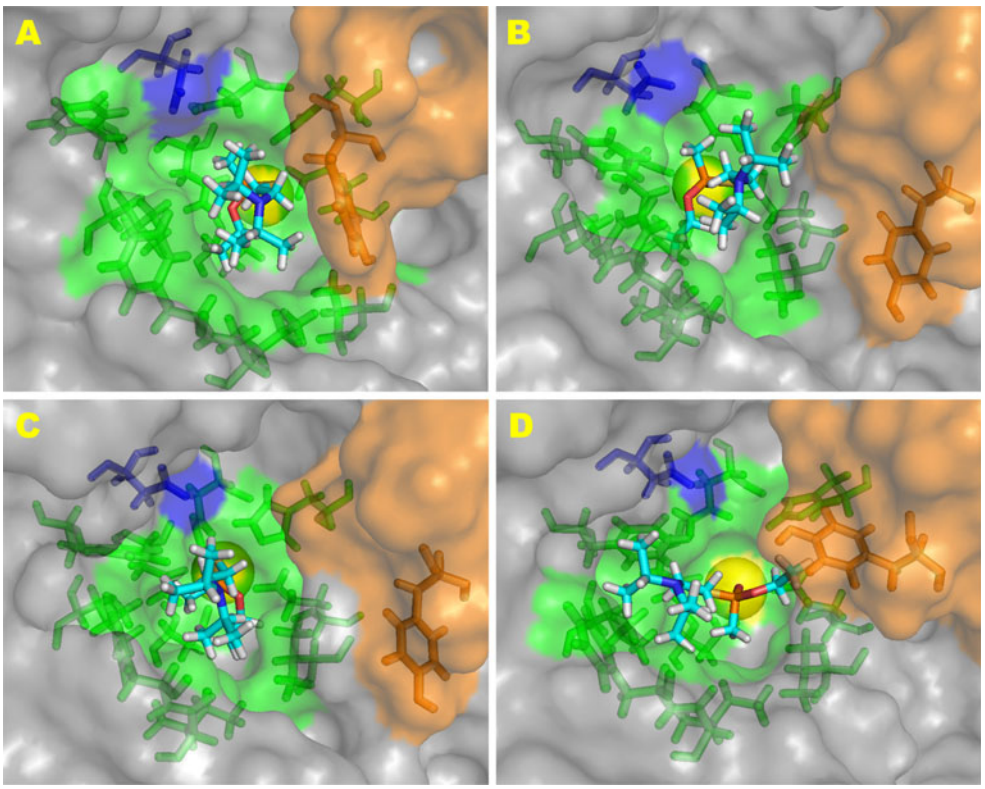

Fig. 5 Bound conformations of VX in HuPON1's active site as predicted by steered molecular dynamics (**a**), DOCK (**b**), FRED (**c**), and AutoDock (**d**). HuPON1 is shown as a semi-transparent gray surface. Residue D183 is highlighted in blue, residues 69 through 82 in orange, and key residues identified in this study in green (E53, H115, N168, F222, N224, L240, D269, I291, F292, and V346). Stick diagrams are also shown for D183 (blue), the key residues (green), Y71 (orange), and VX (light blue carbon atoms). The active site calcium ion is drawn as a yellow sphere. All images generated in PyMOL [72]

FRED

For the FRED-based structure, E53, N168, N224, and D269 all coordinate the active site calcium. Residues I291, F292, and F222 interact with VX's DPAE group. I291 also forms a partial interaction with VX's O-ethyl group while F222 forms a partial interaction with VX's methyl group. L240 interacts with VX's methyl group, and residues V346, T332, and H285 all interact with VX's O-ethyl moiety. In the FRED structure, H115 is situated directly behind the methyl group on VX's phosphorus atom along the P-S bond. As with the DOCK and SMD structures, this conformation would prevent H115 from coordinating a water molecule for hydrolyzing VX's P-S bond. Interactions of key residues and water molecules were further characterized through an MD simulation of the bound FRED structure. The results show that VX maintains close contact with L240, H285, F292, V346, and I291. The MD-simulations also revealed that the interaction of F292 with VX's DPAE group is a dipole-quadrup ole interaction.

AutoDock

Despite its rotated orientation, the AutoDock-based structure still maintains many interactions found in other docking predictions. For example, H184, M196, F222, L240, L241, I291, and F292 all interact with VX's hydrophobic DPAE group, with many of these same interactions being observed in other bound structures (Table 1). T332 and V346 both interact with VX's methyl group, while E53, Y71, H115, and V346 all interact with VX's O-ethyl group. As expected, E53 and D269 coordinate the active site calcium ion. Further, H115 is located behind VX's phosphorus atom inline with the methyl group attached to the phosphorus. Thus, none of the four bound conformations for VX has H115 in an ideal position for directly coordinating a water-based SN2 attack of VX's P-S bond.

Key residue localization

Figure 5 illustrates the localization of HuPON1 residues associated with VX binding to HuPON1. As the figure demonstrates, the four VX binding conformations have some variation in their positioning within HuPON1's active site. However, as previously discussed, it is likely that the HuPON1-VX system could readily move between the different bound conformations. Further, Fig. 5 shows that the ten key residues identified in this study (E53, H115, N168, F222, N224, L240, D269, I291, F292, and V346) are consistently found near VX across all the bound conformations. Figure 5 also demonstrates that the key residues are located opposite of the loop region that was missing from rPON1's structure (i.e., the loop containing residues 72 through 79). This localization of the key residues supports a binding mechanism where HuPON1's flexible loop region acts as a gatekeeper to the active site residues required for binding VX.

Along with the key residues, Fig. 5 also illustrates the location of D183 in each bound conformation. Given D183's predicted pKa and its localization within HuPON1's active site, it is possible that D183 could serve as a proton donor or acceptor during HuPON1 hydrolysis reactions. For example, the proximity of VX's sulfur atom to D183's sidechain oxygen atoms in the FRED-based binding prediction of VX illustrates that D183 could potentially serve as a proton to VX's sulfur atom following cleavage of VX's P-S bond.

Solvated interaction energy

Using the SIE method, the SMD, DOCK, FRED and AutoDock structures have calculated binding free energies of −6.20 kcal/mol (σ=0.28 kcal/mol), −6.31 kcal/mol (σ= 0.29 kcal/mol), −6.25 kcal/mol (σ=0.34 kcal/mol), and −6.24 kcal/mol (σ=0.35 kcal/mol), respectively. The average SIE values are all very close and well within each other's standard deviations. This indicates that VX may be able to readily move between the different predicted bound conformations while maintaining the interaction between its lone oxygen atom and the active site calcium ion.

Protonated VX binding predictions

In addition to running binding simulations between HuPON1 and the neutral form of VX, we also tested the binding predictions between HuPON1 and the protonated form of VX (data not shown). These binding simulations were performed using AutoDock, DOCK, and FRED with subsequent equilibration through molecular dynamics. All parameters and procedures were equivalent to those used for the neutral form of VX. Across all three prediction methods, the binding conformations with the protonated state of VX were consistent with those for the neutral state. In particular, the lone oxygen on VX's phosphorus atom was always found to interact directly with HuPON1's active site calcium ion. Further, the groups attached to VX's phosphorus atom displayed a range of conformations consistent with those found for the neutral state. Additionally, VX's 2DPAE group was found to be oriented outward from HuPON1's active site. Finally, we analyzed the key residues for the bound conformations of protonated VX using the distance measure described previously. The following residues were found to interact with VX in all three bound conformations: H115, N168, F222, N224, D269, H285, I291, T332, V346, and F347. Additionally, residues E53, L240, and F292 were found to interact with

VX in two of the three conformations, while K75, H134 and H184 were found to interact with VX in one of the three conformations. These results are in good agreement with the results listed in Table 1 for the neutral state. Altogether, the binding results do not change significantly when VX is modeled in the protonated state.

Summary

We have characterized the three-dimensional structure of the human serum paraoxonase 1 (HuPON1) protein and its binding mechanism to the S-enantiomer of VX. Three-dimensional structures were determined through two different approaches, providing alternate models for the region missing from the crystal structure of rPON1. Docking simulations with VX were then performed using AutoDock, DOCK, FRED, and SMD followed by molecular dynamics simulations. For all four studies, VX's lone oxygen atom formed a direct interaction with HuPON1's active site calcium ion, and VX's (diisopropylamino)ethyl group was situated toward the outer part of HuPON1's active site. The DOCK and SMD conformations had similar positioning of VX and the P-S bond in the active site, while the FRED and AutoDock structures were rotated approximately 90° and 180° counterclockwise along the P-Ca^{2+} torsional axis, respectively, relative to the DOCK and SMD structures. The fact that the SMD binding simulations with a closed HuPON1 conformation matched static binding procedures with an open conformation shows SMD binding simulations can be useful for obtaining binding predictions even when starting with a protein structure in a closed conformation. SIE analysis revealed that all four conformations have nearly identical binding energies, indicating that VX may readily move between the different bound conformations. Analysis of residues within 3 Å of each bound structure showed that E53, H115, N168, F222, N224, L240, D269, I291, F292, and V346 all form interactions with VX, matching with predictions made by FTMAP.

Regarding HuPON1's catalytic mechanism for VX degradation, no bound structure was found where H115, a putative catalytic residue, can directly facilitate a water-based SN2 attack of VX's P-S bond at the phosphorus atom. However, three of the predicted binding conformations have VX's P-S bond aligned with residue D269. This is consistent with a proposed mechanism where D269 serves as catalytic residue for HuPON1 hydrolysis reactions [71]. Additionally, one predicted binding conformation has VX's P-S bond aligned with E53, raising the possibility that E53 could potentially serve as a catalytic residue. Further, given that all the predicted binding conformations have similar binding energies (based on SIE calculations) and are structurally similar, the results from this study are also consistent with a proposed mechanism where a water molecule loses a proton to one of many bases within HuPON1's active site prior to the resulting hydroxide ion attacking the substrate [70].

While the binding results do not offer conclusive evidence on HuPON1's hydrolysis mechanism for VX, they do illustrate various aspects of VX's binding mechanism prior to hydrolysis. The results show that VX's lone oxygen atom has a strong preference for interacting directly with HuPON1's active site calcium. Additionally, the binding predictions suggest that VX can have a range of rotations within HuPON1's active site with these different conformations having similar predicted binding energies. Across this range, VX is able to maintain proximity to a set of key residues near the active site calcium. These key residues are located opposite from HuPON1's flexible loop region, with the flexible loop potentially serving as a gatekeeper for VX binding. Additionally, residue D183's location and predicted pKa indicate that this residue could potentially serve as a proton donor or acceptor during VX hydrolysis. Altogether, the results provide insight into how HuPON1 can interact with VX and reveal potential mutagenesis targets for enhancing HuPON1's VX hydrolase activity.

Supporting material available

The supporting material includes PDB files for the I-TASSER and MODELLER-based predictions of HuPON1's tertiary structure. The supporting material also includes PDB files for the bound HuPON1-VX structures based on binding predictions by AutoDock, DOCK, FRED, and SMD followed by MD simulations.

Acknowledgements This research was supported by the Defense Threat Reduction Agency-Joint Science and Technology Office, Medical S&T Division. The opinions, interpretations, conclusions, and recommendations are those of the authors and are not necessarily endorsed by the U.S. Army or the Department of Defense.

References

1. Newmark J (2007) Nerve agents. Neurologist 13(1):20–32
2. Yokoyama K, Yamada A, Mimura N (1996) Clinical profiles of patients with sarin poisoning after the Tokyo subway attack. Am J Med 100(5):586
3. Cannard K (2006) The acute treatment of nerve agent exposure. J Neurol Sci 249(1):86–94
4. Rastogi SK, Wenger GR, Mcmillan DE (1985) Effects of optical isomers of pentobarbital on behavior in rats maintained on either the D or the L optical isomer of methadone. Arch Int Pharmacodyn Ther 276(2):247–262
5. Kuo CL, La Du BN (1998) Calcium binding by human and rabbit serum paraoxonases-structural stability and enzymatic activity. Drug Metab Dispos 26(7):653–660

6. Yeung DT, Lenz DE, Cerasoli DM (2005) Analysis of active-site amino-acid residues of human serum paraoxonase using competitive substrates. FEBS J 272(9):2225–2230
7. Rochu D, Chabriere E, Masson P (2007) Human paraoxonase: a promising approach for pre-treatment and therapy of organophosphorus poisoning. Toxicology 233(1–3):47–59
8. Draganov DI, Teiber JF, Speelman A, Osawa Y, Sunahara R, La Du BN (2005) Human paraoxonases (PON1, PON2, and PON3) are lactonases with overlapping and distinct substrate specificities. J Lipid Res 46(6):1239–1247
9. Khersonsky O, Tawfik DS (2005) Structure-reactivity studies of serum paraoxonase PON1 suggest that its native activity is lactonase. Biochemistry 44(16):6371–6382
10. Josse D, Lockridge O, Xie WH, Bartels F, Schopfer LM, Masson P (2001) The active site of human paraoxonase (PON1). J Appl Toxicol 21(suppl 1):S7–S11
11. Yeung DT, Josse D, Nicholson JD, Khanal A, McAndrew CW, Bahnson BJ, Lenz DE, Cerasoli DM (2004) Structure/function analyses of human serum paraoxonase (HuPON1) mutants designed from a DFPase-like homology model. BBA-Proteins Proteomics 1702(1):67–77
12. Hu X, Jiang X, Lenz DE, Cerasoli DM, Wallqvist A (2009) In silico analyses of substrate interactions with human serum paraoxonase 1. Proteins 75(2):486–498
13. Harel M, Aharoni A, Gaidukov L, Brumshtein B, Khersonsky O, Meged R, Dvir H, Ravelli RBG, McCarthy A, Toker L, Silman I, Sussman JL, Tawfik DS (2004) Structure and evolution of the serum paraoxonase family of detoxifying and anti-atherosclerotic enzymes. Nat Struct Mol Biol 11(5):412–419
14. Lee MS, Yeh I, Zavajevski N, Wilson P, Reifman J (2006) A software pipeline for protein structure prediction. In Proceedings of the 25th Army Science Conference, Orlando, FL
15. Zhang Y (2008) I-TASSER server for protein 3D structure prediction. BMC Bioinformatics 9:40
16. Zhang Y (2007) Template-based modeling and free modeling by I-TASSER in CASP7. Proteins 69(suppl 8):108–117
17. Sali A, Blundell TL (1993) Comparative protein modeling by satisfaction of spatial restraints. J Mol Biol 234(3):779–815
18. Fiser A, Do RKG, Sali A (2000) Modeling of loops in protein structures. Protein Sci 9(9):1753–1773
19. Moustakas DT, Lang PT, Pegg S, Pettersen E, Kuntz ID, Brooijmans N, Rizzo RC (2006) Development and validation of a modular, extensible docking program: DOCK5. J Comput-Aided Mol Des 20(10-11):601–619
20. Morris GM, Goodsell DS, Halliday RS, Huey R, Hart WE, Belew RK, Olson AJ (1998) Automated docking using a Lamarckian genetic algorithm and an empirical binding free energy function. J Comput Chem 19(14):1639–1662
21. Huey R, Morris GM, Olson AJ, Goodsell DS (2007) A semiempirical free energy force field with charge-based desolvation. J Comput Chem 28(6):1145–1152
22. McGann MR, Almond HR, Nicholls A, Grant JA, Brown FK (2003) Gaussian docking functions. Biopolymers 68(1):76–90
23. OEChem, version 1.3.4 (2005) OpenEye Scientific Software, Inc., Santa Fe, NM, USA, www.eyesopen.com
24. Osterberg F, Morris GM, Sanner MF, Olson AJ, Goodsell DS (2002) Automated docking to multiple target structures: incorporation of protein mobility and structural water heterogeneity in AutoDock. Proteins 46(1):34–40
25. Pavani P, Mangala SD, Murthy JVVS, Babu AP (2008) Protein-ligand interaction studies on 2, 4, 6-trisubstituted triazine derivatives as antimalarial DHFR agents using AutoDock. Res J Biotechnol 3(3):18–23
26. Zheng F, Yang W, Ko MC, Liu J, Cho H, Gao D, Tong M, Tai HH, Woods JH, Zhan CG (2008) Most efficient cocaine hydrolase designed by virtual screening of transition states. J Am Chem Soc 130(36):12148–12155
27. Tavori H, Khatib S, Aviram M, Vaya J (2008) Characterization of the PON1 active site using modeling simulation, in relation to PON1 lactonase activity. Bioorg Med Chem 16(15):7504–7509
28. Guvench G, MacKerell AD Jr (2009) Computational evaluation of protein-small molecule binding. Curr Opin Struct Biol 19(1):56–61
29. Naim M, Bhat S, Rankin KN, Dennis S, Chowdhury SF, Siddiqi I, Drabik P, Sulea T, Bayly CI, Jakalian A, Purisima EO (2007) Solvated interaction energy (SIE) for scoring protein-ligand binding affinities. 1. Exploring the parameter space. J Chem Inf Model 47(1):122–133
30. Cui Q, Sulea T, Schrag JD, Munger C, Hung MN, Naim M, Cygler M, Purisima EO (2008) Molecular dynamics-solvated interaction energy studies of protein-protein interactions: The MP1-p14 scaffolding complex. J Mol Biol 379(4):787–802
31. Izrailev S, Stepaniants S, Isralewitz B, Kosztin D, Lu H, Molnar F, Wriggers W, Schulten K (1998) Steered molecular dynamics. In: Deuflhard P, Hermans J, Leimkuhler B, Mark AE, Reich S, Skeel RD (eds) Computational molecular dynamics: challenges, methods, ideas. Lecture notes in computational science and engineering vol 4. Springer, Berlin, pp 39–65
32. Benson DA, Karsch-Mizrachi I, Lipman DJ, Ostell J, Wheeler DL (2008) GenBank. Nucleic Acids Res 36(Sp. Iss. SI):D25–D30
33. Gaidukov L, Tawfik DS (2005) High affinity, stability, and lactonase activity of serum paraoxonase PON1 anchored on HDL with ApoA-I. Biochemistry 44(35):11843–11854
34. Gordon JC, Myers JB, Folta T, Shoja V, Heath LS, Onufriev A (2005) H++: a server for estimating pKas and adding missing hydrogens to macromolecules. Nucleic Acids Res 33(suppl 2): W368–W371
35. Anandakrishnan R, Onufriev A (2008) Analysis of basic clustering algorithms for numerical estimation of statistical averages in biomolecules. J Comput Biol 15(2):165–184
36. Case DA, Cheatham TE, Darden T, Gohlke H, Luo R, Merz KM, Onufriev A, Simmering C, Wang B, Woods RJ (2005) The Amber biomolecular simulation programs. J Comput Chem 26(16):1668–1688
37. Hornak V, Abel R, Okur A, Strockbine B, Roitberg A, Simmerling C (2006) Comparison of multiple amber force fields and development of improved protein backbone parameters. Proteins: Struct Funct Bioinf 65(3):712–725
38. Hawkins GD, Cramer CJ, Truhlar DG (1995) Pairwise solute descreening of solute charges from a dielectric medium. Chem Phys Lett 246(1–2):122–129
39. Hawkins GD, Cramer CJ, Truhlar DG (1996) Parametrized models of aqueous free energies of solvation based on pairwise descreening of solute atomic charges from a dielectric medium. J Phys Chem 100(51):19824–19839
40. Jorgensen WL (1981) Quantum and statistical mechanical studies of liquids. 10. transferable intermolecular potential functions for water, alcohols, and ethers. Application to liquid water. J Am Chem Soc 103(2):335–340
41. Laskowski RA, Macarthur MW, Moss DS, Thornton JM (1993) PROCHECK: a program to check the stereochemical quality of protein structures. J Appl Crystallogr 26(Part 2):283–291
42. Morris AL, Macarthur MW, Hutchinson EG, Thornton JM (1992) Stereochemical quality of protein-structure coordinates. Proteins 12(4):345–364
43. Marti-Renom MA, Stuart AC, Fiser A, Sanchez R, Melo F, Sali A (2000) Comparative protein structure modeling of genes and genomes. Annu Rev Biophys Biom 29:291–325
44. Wang JM, Cieplak P, Kollman PA (2000) How well does a restrained electrostatic potential (RESP) model perform in calculating conformational energies of organic and biological molecules? J Comput Chem 21(12):1049–1074
45. Ordentlich A, Barak D, Sod-Moriah G, Kaplan D, Mizrahi D, Segall Y, Kronman C, Karton Y, Lazar A, Marcus D, Velan B, Shafferman A (2005) The role of AChE active site gorge in

determining stereoselectivity of charged and noncharged VX enantiomers. Chem Biol Interact 157(Sp. Iss. SI):191–198
46. Anderson E, Veith GD, Weininger D (1987) Smiles: a line notation and computerized interpreter for chemical structures. Technical report U.S. EPA, Environmental Research Laboratory, Duluth, MN
47. http://cactus.nci.nih.gov/services/translate/
48. Jakalian A, Bush BL, Jack DB, Bayly CI (2000) Fast, efficient generation of high-quality atomic charges. AM1-BCC model: I. Method. J Comput Chem 21(2):132–146
49. Jakalian A, Jack DB, Bayly CI (2002) Fast, efficient generation of high-quality atomic charges. AM1-BCC model: II. Parameterization and validation. J Comput Chem 23(16):1623–1641
50. Frisch MJ, Trucks GW, Schlegel HB, Scuseria GE, Robb MA, Cheeseman JR, Mont-gomery JA Jr, Vreven T, Kudin KN, Burant JC, Millam JM, Iyengar SS, Tomasi J, Barone V, Mennucci B, Cossi M, Scalmani G, Rega N, Petersson GA, Nakatsuji H, Hada M, Ehara M, Toyota K, Fukuda R, Hasegawa J, Ishida M, Nakajima T, Honda Y, Kitao O, Nakai H, Klene M, Li X, Knox JE, Hratchian HP, Cross JB, Bakken V, Adamo C, Jaramillo J, Gomperts R, Stratmann RE, Yazyev O, Austin AJ, Cammi R, Pomelli C, Ochterski JW, Ayala PY, Morokuma K, Voth GA, Salvador P, Dannenberg JJ, Zakrzewski VG, Dapprich S, Daniels AD, Strain MC, Farkas O, Malick DK, Rabuck AD, Raghavachari K, Foresman JB, Ortiz JV, Cui Q, Baboul AG, Clifford S, Cioslowski J, Ste-fanov BB, Liu G, Liashenko A, Piskorz P, Komaromi I, Martin RL, Fox DJ, Keith T, Al-Laham MA, Peng CY, Nanayakkara A, Challacombe M, Gill PMW, Johnson B, Chen W, Wong MW, Gonzalez C, Pople JA (2004) Gaussian 03, Revision C.02. Gaussian, Inc, Wallingford, CT
51. Cieplak P, Cornell WD, Bayly C, Kollman PA (1995) Application of the multimolecule and multiconformational RESP methodology to biopolymers-charge derivation for DNA, RNA, and proteins. J Comp Chem 16(11):1357–1377
52. Bayly CI, Cieplak P, Cornell WD, Kollman PA (1993) A well-behaved electrostatic potential based method using charge restraints for deriving atomic charges-the RESP model. J Phys Chem 97(40):10269–10280
53. Case DA, Darden TA, Cheatham TE, Simmerling CL, Wang J, Duke RE, Luo R, Merz KM, Pearlman DA, Crowley M, Walker RC, Zhang W, Wang B, Hayik S, Roitberg A, Seabra G, Wong KF, Paesani F, Wu X, Brozell S, Tsui V, Gohlke H, Yang L, Tan C, Mongan J, Hornak V, Cui G, Beroza P, Mathews DH, Schafmeister C, Ross WS, Kollman PA (2006) AMBER 10. University of California, San Francisco
54. Marsili M, Gasteiger J (1980) Pi-charge distributions from molecular topology and pi-orbital electronegativity. Croat Chem Acta 53:601–614
55. Marsili M, Gasteiger J (1980) Iterative partial equalization of orbital electronegativity-a rapid access to atomic charges. Tetrahedron 36:3219–3228
56. Sanner MF (1999) Python: a programming language for software integration and development. J Mol Graphics Mod 17:57–61
57. Pettersen EF, Goddard TD, Huang CC, Couch GS, Greenblatt DM, Meng EC, Ferrin TE (2004) UCSF chimera-a visualization system for exploratory research and analysis. J Comput Chem 25 (13):1605–1612
58. Richards FM (1977) Areas, volumes, packing and protein structure. Annu Rev Biophys Bioeng 6:151–176
59. Harvey SC (1989) Treatment of electrostatic effects in macromolecular modeling. Proteins 5(1):78–92
60. Guenot J, Kollman PA (1992) Molecular-dynamics studies of a DNA-binding protein: 2. An evaluation of implicit and explicit solvent models for the molecular-dynamics simulation of the Escherichia-coli trp repressor. Protein Sci 1(9):1185–1205
61. Pan YM, Gao DQ, Yang WC, Cho H, Yang GF, Tai HH, Zhan CG (2005) Computational redesign of human butyrylcholinesterase for anticocaine medication. Proc Natl Acad Sci USA 102 (46):16656–16661
62. Zhang T, Hamza A, Cao X, Wang B, Yu S, Zhan CG, Sun D (2008) A novel Hsp90 inhibitor to disrupt Hsp90/Cdc37 complex against pancreatic cancer cells. Mol Cancer Ther 7(1):162–170
63. Bargagna-Mohan P, Hamza A, Kim Y, Ho YK, Mor-Valknin N, Wendschlag N, Li J, Evans RM, Markovitz DM, Zhan CG, Kim KB, Mohan R (2007) The tumor inhibitor and antiangiogenic agent withaferin A targets the intermediate filament protein vimentin. Chem Biol 14(6):623–634
64. Guex N, Peitsch MC (1997) SWISS-MODEL and the Swiss-PdbViewer: an environment for comparative protein modeling. Electrophoresis 18(15):2714–2723
65. Kollman PA, Massova I, Reyes C, Kuhn B, Huo SH, Chong L, Lee M, Lee T, Duan Y, Wang W, Donini O, Cieplak P, Srinivasan J, Case DA, Cheatham TE (2000) Calculating structures and free energies of complex molecules: combining molecular mechanics and continuum models. Accounts Chem Res 33(12):889–897
66. Brenke R, Kozakov D, Chuang GY, Beglov D, Hall D, Landon MR, Mattos C, Vajda S (2009) Fragment-based identification of druggable 'hot spots' of proteins using Fourier domain correlation techniques. Bioinformatics 25(5):621–627
67. Kortvelyesi T, Dennis S, Silberstein M, Brown L, Vajda S (2003) Algorithms for computational solvent mapping of proteins. Proteins 51(3):340–351
68. Silberstein M, Dennis S, Brown L, Kortvelyesi T, Clodfelter K, Vajda S (2003) Identification of substrate binding sites in enzymes by computational solvent mapping. J Mol Biol 332(5):1095–1113
69. Blum MM, Timperley CM, Williams GR, Thiermann H, Worek F (2008) Inhibitory potency against human acetylcholinesterase and enzymatic hydrolysis of fluorogenic nerve agent mimics by human paraoxonase 1 and squid diisopropyl fluorophosphatase. Biochemistry 47(18):5216–5224
70. Khersonsky O, Tawfik DS (2006) The histidine 115-histidine 134 dyad mediates the lactonase activity of mammalian serum paraoxonases. J Biol Chem 281(11):7649–7656
71. Blum MM, Löhr F, Richardt A, Rüterjans H, Chen JCH (2006) Binding of a designed substrate analogue to diisopropyl fluorophosphatase: Implications for the phosphotriesterase mechanism. J Am Chem Soc 128(39):12750–12757
72. DeLano WL (2002) The PyMOL molecular graphics system. http://www.pymol.org